ARMY RESEARCH LABORATORY

Characterization of Energetic Porous Silicon for a Microelectromechanical System (MEMS)-Based Solid Propellant Microthruster

by Raghav Ramachandran, Wayne Churaman, David Lunking, and Christopher J Morris

ARL-TR-7087 **September 2014**

NOTICES

Disclaimers

The findings in this report are not to be construed as an official Department of the Army position unless so designated by other authorized documents.

Citation of manufacturer's or trade names does not constitute an official endorsement or approval of the use thereof.

Destroy this report when it is no longer needed. Do not return it to the originator.

Army Research Laboratory
Adelphi, MD 20783-1138

ARL-TR-7087 **September 2014**

Characterization of Energetic Porous Silicon for a Microelectromechanical System (MEMS)-Based Solid Propellant Microthruster

Raghav Ramachandran, Wayne Churaman, David Lunking, and Christopher J Morris
Sensors and Electron Devices Directorate, ARL

REPORT DOCUMENTATION PAGE	Form Approved OMB No. 0704-0188

PLEASE DO NOT RETURN YOUR FORM TO THE ABOVE ADDRESS.

1. REPORT DATE *(DD-MM-YYYY)*	2. REPORT TYPE	3. DATES COVERED (From - To)
September 2014	Final	

4. TITLE AND SUBTITLE

Characterization of Energetic Porous Silicon for a Microelectromechanical System (MEMS)-Based Solid Propellant Microthruster

5a. CONTRACT NUMBER

5b. GRANT NUMBER

5c. PROGRAM ELEMENT NUMBER

6. AUTHOR(S)

Raghav Ramachandran, Wayne Churaman, David Lunking, and Christopher J Morris

5d. PROJECT NUMBER

5e. TASK NUMBER

5f. WORK UNIT NUMBER

7. PERFORMING ORGANIZATION NAME(S) AND ADDRESS(ES)

US Army Research Laboratory
ATTN: RDRL-SER-L
2800 Powder Mill Road
Adelphi, MD 20783-1138

8. PERFORMING ORGANIZATION REPORT NUMBER

ARL-TR-7087

9. SPONSORING/MONITORING AGENCY NAME(S) AND ADDRESS(ES)

10. SPONSOR/MONITOR'S ACRONYM(S)

11. SPONSOR/MONITOR'S REPORT NUMBER(S)

12. DISTRIBUTION/AVAILABILITY STATEMENT

Approved for public release; distribution unlimited.

13. SUPPLEMENTARY NOTES

14. ABSTRACT

Silicon can be converted into porous silicon (PS) through a galvanic etch process and then rendered energetic when infused with any one of a number of oxidizers. Energetic PS can provide variable energy release to generate thrust and the displacement of small-scale devices such as microthrusters and micro-satellites. In this report, we investigate the etch process and its repeatability for pore formation during etches. We found that using a fresh etch bath reduces variability in pore characteristics. In addition, we examine the thrust output of a combustion reaction of PS activated with sodium perchlorate. Experimental testing showed that the forces ranged from tens to hundreds of millinewtons, depending on the silicon wafer resistivity and pore morphology, which is controlled by the etch parameters.

15. SUBJECT TERMS

porous silicon, combustion, nanoenergetics, microthrusters

16. SECURITY CLASSIFICATION OF:			17. LIMITATION OF ABSTRACT	18. NUMBER OF PAGES	19a. NAME OF RESPONSIBLE PERSON
A. Report	b. ABSTRACT	c. THIS PAGE			Christopher J Morris
Unclassified	Unclassified	Unclassified	UU	24	19b. TELEPHONE NUMBER (*Include area code*) (301) 394-0950

Standard Form 298 (Rev. 8/98)
Prescribed by ANSI Std. Z39.18

Contents

List of Figures

List of Tables

INTENTIONALLY LEFT BLANK.

1. Introduction

Porous silicon (PS) emerged as energetic material in 1992, when it was discovered that nitric acid mixed with PS results in an explosive reaction. Further experiments in 2001 validated the exothermic release of energy when PS reacted with oxygen at cryogenic temperatures. These reactions were due to the oxidization of silicon, which results in a high energy release comparable to traditional carbon-hydrogen-nitrogen-oxygen (CHNO) based explosives.[1] With the advent of microelectromechanical systems (MEMS) and bulk micromachining techniques, efforts to integrate micrometer-scale, solid-state explosives onto silicon wafers were made in order to demonstrate future applications such as actuation and propulsion.[2,3]

In recent years, various technological efforts have been made to develop micro-propulsion systems for actuation. Two types of MEMS-based micro-propulsion devices have been the focus for MEMS fabrication and integration: vaporizing liquid thrusters and solid propellant thrusters. Vaporizing liquid thrusters involve a fabricated chamber with a fluidic inlet and nozzle exit micromachined onto a silicon substrate. The heating of the chamber results in a vaporization, which creates thrust. While liquid thrusters can provide variable thrust continuously, their thrust-to-power ratios are low as they require large amounts of power to heat the chamber. Because silicon is characterized by high thermal conductivity, the chamber needs to be sealed with an insulating material.[4] Solid propellant thrusters involve the fabrication of a solid fuel, such as PS, as a part of a micromachined device on a silicon substrate. As the propellant is ignited, thrust is generated. The advantages to such thrusters are the low power required for ignition and the avoidance of leakage. The major drawbacks are the inability to restart or easily reload a single region of propellant. This drawback can be partially overcome by creating an array of propellants.[5]

In this work, we characterize energetic PS in an intended microthruster device. Thrust and specific impulse as a function of pore morphology are examined. With a constant etch depth and wafer resistivity, a 3:1 etch concentration results in a higher thrust output than a 20:1 etch concentration. With a constant etch depth and concentration, a thruster from a 5.5 ohm-cm wafer generates larger thrusts than those of low resistivity. While the refreshment of an etch bath initially indicated a more repeatable pore morphology, more tests need to be conducted in order to validate this claim.

2. Fabrication

Details of the microthruster fabrication process are covered in a published paper.[6] Briefly, a nitride layer is coated on one side of the wafer, while platinum is sputter deposited on to the other side. Devices are then lithographically patterned onto the nitride layer. After patterning is complete, the wafer can be diced into several coupons, or arrays of silicon pixels. The exposed silicon region on the chip is etched using a galvanic process, which involves a mixture of hydrofluoric acid (HF) and ethanol (EtOH), with 2.4 % hydrogen peroxide. With the coupons used on a force sensor, a bridge wire connects the silicon pixels to the bond pads, where an electrical wire can be soldered. The coupons used for volumetric analysis consisted of a bridge wire connecting across a row of millimeter-diameter silicon pixels. It should be noted that a microthruster coupon typically consists of a 2x2 array of pixels. Figure 1 illustrates the etching process.

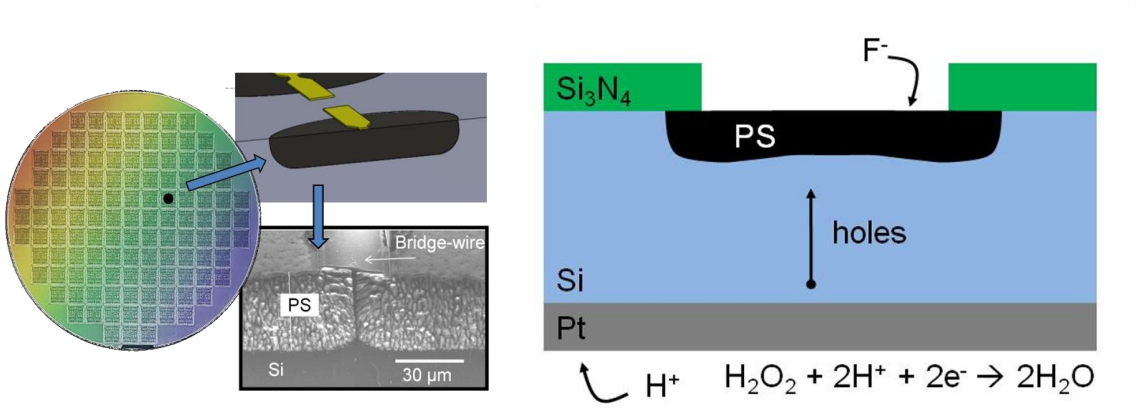

Fig. 1 Illustration of etching process

3. Test Methodology

In order to evaluate the force and specific impulse of energetic PS, an experimental setup was developed using a Kistler 9215 force sensor, as shown in Fig. 2. This piezoelectric sensor contains an external thread and an M2 tap where the microthruster can be attached using an adhesive. Wires are soldered to the bond pads of the thruster, and leads from a voltage supply can be attached to provide ignition. An amplifier converts the sensor signal into a voltage signal that is measured by an oscilloscope. The voltage output can be converted back into a force based on an amplifier gain setting. The amplifier generates a set number of newtons per volt measured. When properly mounted to the M2 tap, 6 µL of sodium perchlorate dissolved in methanol

(3.2 M) are applied to the PS. The sample is dried for 30 min before ignition. In these experiments, we used 2-mm-diameter PS samples with PS layers approximately 30 µm deep. The two parameters studied were the resistivity of the silicon wafers and the HF:EtOH etch ratio.

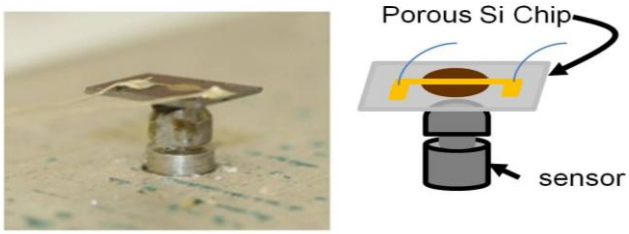

Fig. 2 Image of a PS-based microthruster

Volumetric analysis using the Brunauer, Emmett, Teller (BET) method measures gas adsorption into PS in order to determine the pore characteristics. The coupon used in BET testing contained a 5x5 array, or a total of 25 silicon pixels. A clip was attached to the bottom left corner of the coupon, and then attached to a slotted circular disk. The disk was submerged in the etch bath at a pre-determined location in order to control placement of the coupon during the etch. After etching, the 5x5 array was then cleaved into four usable pieces (as shown in Fig. 3), weighed, and placed in a BET test tube for a 3-h degas cycle. The piece that was in direct contact with the clip was not used in the BET. After analyzing pore characteristics in the BET test, the coupon pieces were dissolved in sodium hydroxide in order to determine the etch depths of the pores as well as total mass of porous material. Figure 3 illustrates how each etched coupon was cleaved.

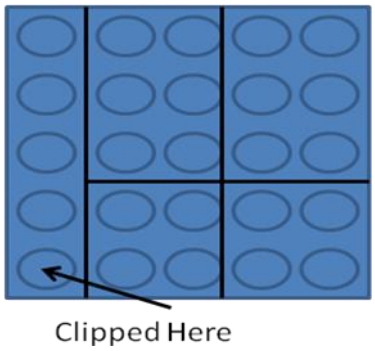

Fig. 3 Diagram of a 5x5 array of silicon pixels

4. Results and Discussion

4.1 Etch Parameters

Initially, when conducting a set of three etches, there were no specific controls for the placement of the coupon, and the etch bath was reused for subsequent etches. Table 1 shows changes in pore characteristics (surface area and porosity) with each repetitive etch. We believe that these results are due to the depletion of hydrogen peroxide in subsequent etching. The rate at which the peroxide is depleted depends on the surface area ratio of exposed silicon to platinum. A second set of three etches was then done with a newly mixed etch bath for each etch and where the coupon was fixed. Table 2 showcases the results from the second set of etches. It appears as though similar pore characteristics can be obtained by refreshing the etch solution and controlling the placement of the coupon.

Table 1 Pore characteristics from an uncontrolled 5-min etch

Conc.	Depth (μm)	SA (m^2/g)	Volume (cm^3/g)	Porosity (%)
3:01	23–30	721.7	0.6768	61.19
3:01	21–23	848.2	0.8079	65.31
3:01	21–24	591.9	0.6384	59.80

Table 2 Pore characteristics from a controlled 5-min etch

Conc.	Depth (μm)	SA (m^2/g)	Volume (cm^3/g)	Porosity (%)
3:01	31–34	968.64	1.22	73.98
3:01	31–34	971.12	1.16	72.99
3:01	31–34	947.35	1.16	72.99

In order to determine porosity as a function of etch time, three sets of etches based on the length of the etch were analyzed using the BET method. Tables 3, 4, and 5 display the pore characteristics that resulted from 5-, 10-, and 15-min etches, respectively. It should be noted that the wafer resistivity of all the coupons used in these tests was either 8.3 or 8.7 ohm-cm. While the pore characteristics were not as consistent through repeated etching as what was shown in Table 3, longer etches indicate less variability for these characteristics.

Table 3 Pore characteristics for a 5-min etch at a 3:1 concentration

Sample	Depth (μm)	SA (m^2/g)	Volume (cm^3/g)	Mass (mg)	Pore Size (nm)	Porosity (%)
1	26.7	1378.13	1.65	0.9	3.28	79.36
2	25.2	1226.71	1.34	1.0	3.07	75.74
3	28.2	1503.89	1.83	1.1	3.32	81.00
4	24.2	1776.19	2.24	0.9	3.43	83.92
5	28.1	656.11	0.47	3.0	2.55	52.27
6	22.6	929.64	1	2.5	3.03	69.97

Table 4 Pore characteristics of a 10-min etch at a 3:1 concentration

Sample	Depth (μm)	SA (m^2/g)	Volume (cm^3/g)	Mass (mg)	Pore Size (nm)	Porosity (%)
1	47.3	1056.17	1.37	2.5	3.47	76.15
2	41.3	1323.96	1.48	1.7	3.14	77.52
3	43.4	1265.13	1.52	1.9	3.29	77.98
4	50.3	882.13	1.15	3.1	3.49	72.82
5	47.4	1027.84	1.33	2.3	3.46	75.60

Table 5 Pore characteristics of a 15-min etch at a 3:1 concentration

Sample	Depth (μm)	SA (m^2/g)	Volume (cm^3/g)	Mass (mg)	Pore Size (nm)	Porosity (%)
1	60.3	1650.03	2.19	2.4	3.54	83.61
2	54.7	869.72	1.01	2.8	3.23	70.18
3	61.6	886.23	1.09	3.4	3.37	71.75
4	63.5	806.50	0.99	6.8	3.38	69.76
5	56.3	870.13	1.06	6.4	3.33	71.18

The greatest display of variability exists with the results associated with a 5-min etch. These etches resulted in the lowest etch depth and mass. The mass recorded on the scale in the lab gives a reading to six decimal places. The BET software, however, truncates an input mass to four decimal places. With a small amount of mass to measure, the BET machine may not be able to provide accurate pore measurements because of a possible rounding error related to the input mass when truncated. An example calculation indicates that changing the mass by a tenth of a milligram decreases the surface area reading by 9%. This could explain why the surface area readings are very large compared to the porosity and the low mass. Samples 5 and 6 from Table 3 used coupons from two separate etches, and lower surface area readings were obtainable because of a larger amount of mass being read through the BET.

As seen in Table 4, the 10-min etches also provided for large surface area readings despite their low mass. With the exception of Sample 4, the porosity readings did not largely vary, although there was still variance related to mass and pore size. As seen in Table 5, the samples related to the 15-min etch showed lower surface area readings and consistent porosity values along with

very slight variances in volume and pore size. It appears that Sample 1 is an outlier and that the other samples may reveal a particular trend. Samples 4 and 5 used coupons from two separate etches, explaining why the mass was larger.

The variations in etch depth could have affected the results shown in the tables above. Referring to Fig. 3, we did not track specific positions at which etch depth measurements were made. However, from a previous experiment, shown in Table 6, the etch depth of a full 5x5 array of 2-mm PS pixels etched for 10 min was measured. Neglecting the corner pixel of column 1, row 1 that was affected by the clip holder, the variation from the center to the edges and corners can be as large as 8%. With the cleaved pieces, many depth measurements were made for both side/corner pixels and inner pixels. For future measurements, specific locations of the array should be identified and recorded to provide better accuracy and consistency. Figure 4 shows a contour plot of the etch depth variation in the 5x5 array.

Table 6 Etch depth (in micrometers) over a 5x5 array of 2-mm PS devices, with percent variation compared to center device

	Column 1	**Column 2**	**Column 3**	**Column 4**	**Column 5**
Row 1	36.3	52.1	52.3	52.3	53.4
Row 2	53.0	50.4	50.0	50.3	52.9
Row 3	52.7	49.6	49.2	49.8	52.8
Row 4	51.6	49.8	49.5	50.0	52.5
Row 5	52.1	51.0	48.7	51.0	51.6
%Variation from Center					
	–26%	6%	6%	6%	8%
	8%	2%	2%	2%	7%
	7%	1%	0%	1%	7%
	5%	1%	0%	2%	7%
	6%	4%	-1%	4%	5%

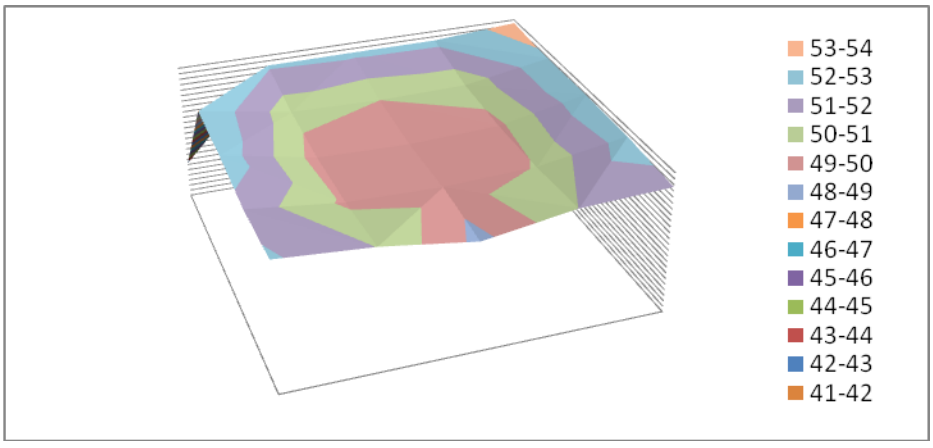

Fig. 4 Contour plot of the etch depth variation in a 5x5 array. The legend shows the etch depth determined in units of micrometers.

The results summarized in Fig. 5 show a general increase in repeatability between measured specific surface area, porosity, and pore size as the etch time increased. The exception was, of course, Sample 1 from Table 5, which exhibited such a high specific surface area for a similar pore size and porosity as compared with other samples from the same set of etch conditions that there may have been an error in mass measurement, BET value calculation, or some combination of others errors. Indeed, such errors may also have been present with the measurements. But with a limited sample size of 4–5 for each case, there seems to be a trend in Fig. 5 that the 15-min etched samples had more repeatable results. If either mass measurement error or BET field entry truncation was a problem, Fig. 5 and the total sample mass values reported in Table 5 suggest a minimum mass of porous material for accurate results to be on the order of 3 mg. Finally, Fig. 6 shows the expected trend that etch depth increased with etch time.

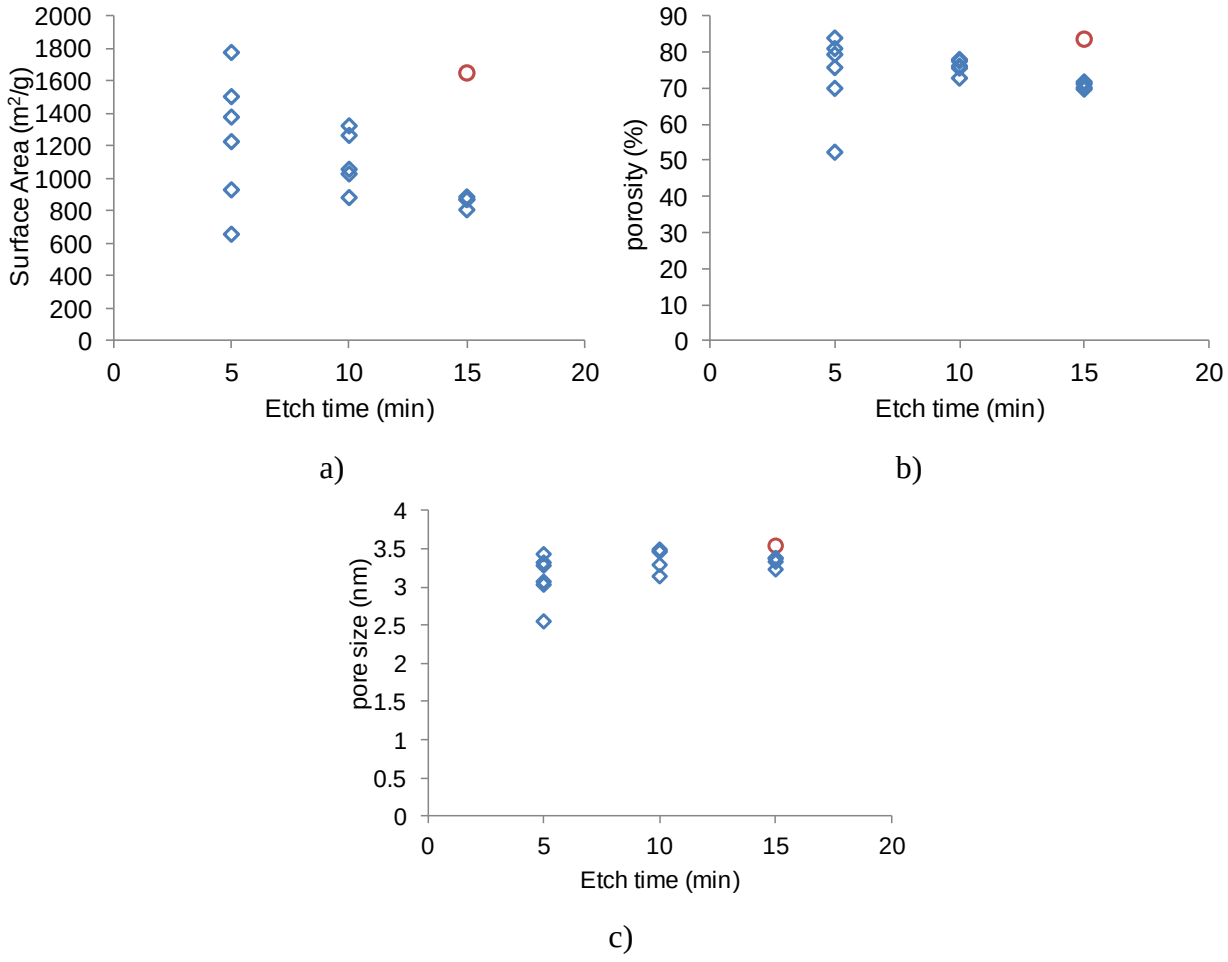

Fig. 5 Specific surface area, porosity, and pore size (data from Tables 3–5) vs. etch time. The red circle in each plot is Sample 1 from Table 5, displayed separately as a possible outlier.

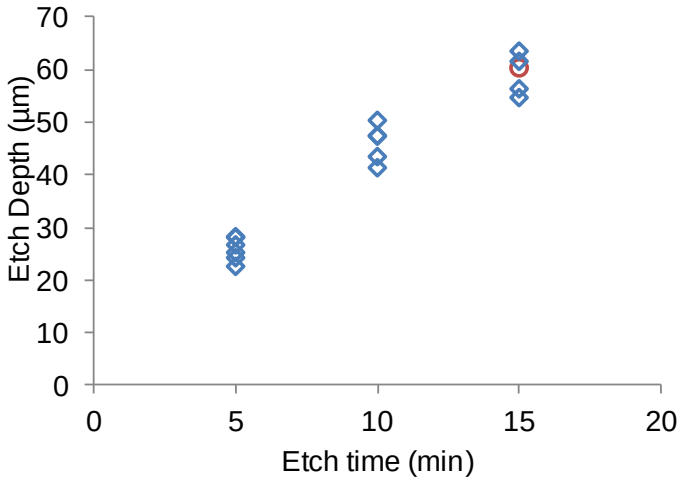

Fig. 6 Etch depth vs. etch time for samples listed in Tables 3–5. As for Fig. 5, the red circle is Sample 1 from Table 5, displayed separately as a possible outlier, although in terms of etch depth it seemed to be within the range of expected variation.

4.2 Force Measurements

Figures 7 and 8 display a total of 10 thruster tests with a 5.5 ohm-cm resistivity wafer etched at a 3:1 concentration. All the thrusters' etch depths were estimated to be 30 microns deep, because all etches were carried out for 6 min. If outliers are taken into consideration, the thrust outputs varied from 200 to 750 mN. Eight of the 10 force curves peaked between 500 and 700 mN. Depth variation could have contributed to the measured thrust variation, but unfortunately depth was not measured for each case. Test numbers 7 and 9, shown in Fig. 8, resulted in an exothermic reaction that broke the corners of each chip, but did not excite resonance in the sensor. This result may have contributed to the different shapes of the thrust versus time curves. A potential reason for the 2nd and 3rd tests in Fig. 7 being much higher and lower in output, respectively, is a variation in drying time of the sodium perchlorate, resulting in different combustion characteristics.

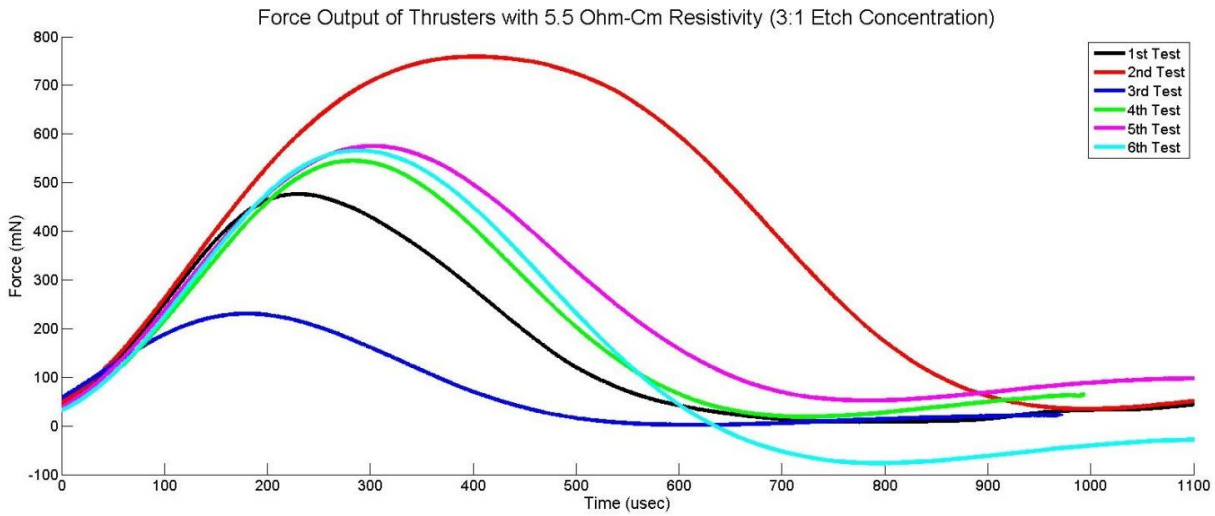

Fig. 7 Output of microthrusters etched at 3:1 ratio with 5.5 ohm-cm resistivity (tests 1–6)

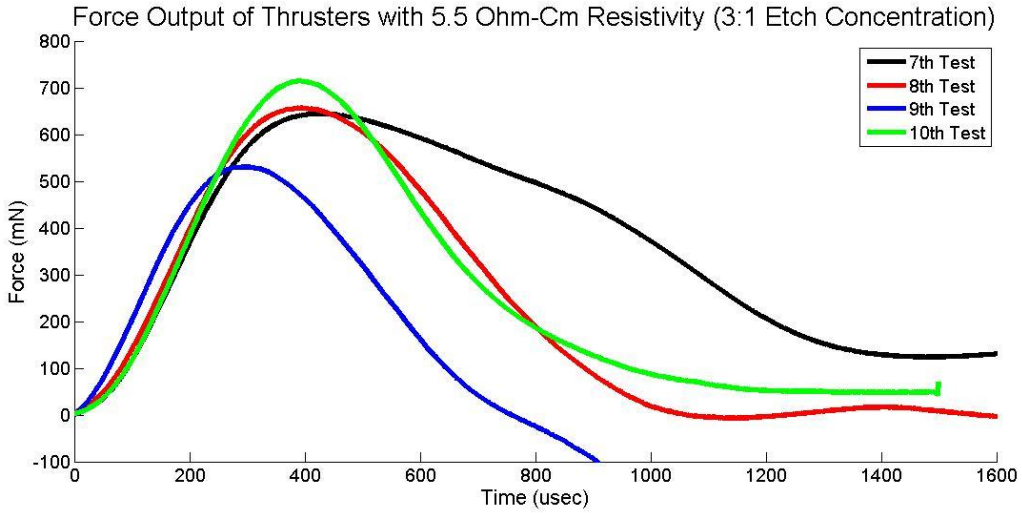

Fig. 8 Output of microthrusters etched at 3:1 ratio with 5.5 ohm-cm resistivity (tests 7–10)

Figure 9 shows more results for a different starting wafer, at 2.29 ohm-cm. It should be noted that the 1st and 2nd test in Fig. 9 correspond to approximately a 40-micron etch depth, while the 3rd and 4th test correspond to a 30-micron depth. The etch duration was 4.5 min for the 40-micron depth and 3 min for the 30-micron depth. Regarding only the two results from Fig. 9 at 30 microns, the peak thrust of the 2.29 ohm-cm devices was 7–25% of the 5.5 ohm-cm devices.

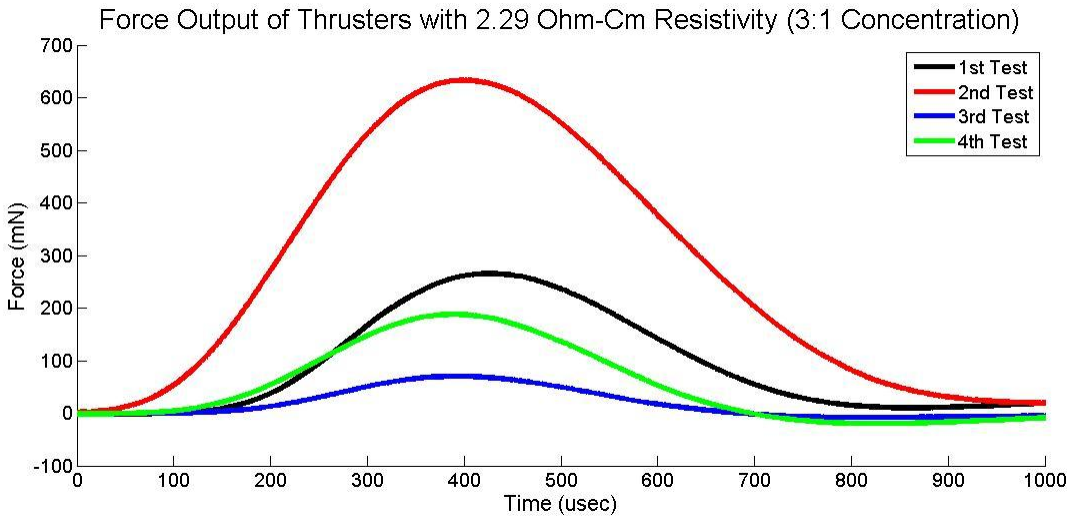

Fig. 9 Output of microthrusters etched at 3:1 ratio with 2.29 ohm-cm resistivity (tests 1–4)

Figures 10 and 11 show the force output for thrusters fabricated with 0.016 ohm-cm resistivity wafers and etched at a 3:1 ratio of HF to EtOH. The thrusters produced forces between 18 and 85 mN. From a limited set of etch depth measurements of several of these devices, deeper etches tended to produce larger forces (i.e., tests 1, 2, and 3). Also, with all seven tests results on a wafer with lower resistivity, the thrust duration appeared to be more consistent, although peak thrust values still varied significantly. The shorter etch times may also have contributed to less variability due to fewer variations in mass across each coupon.

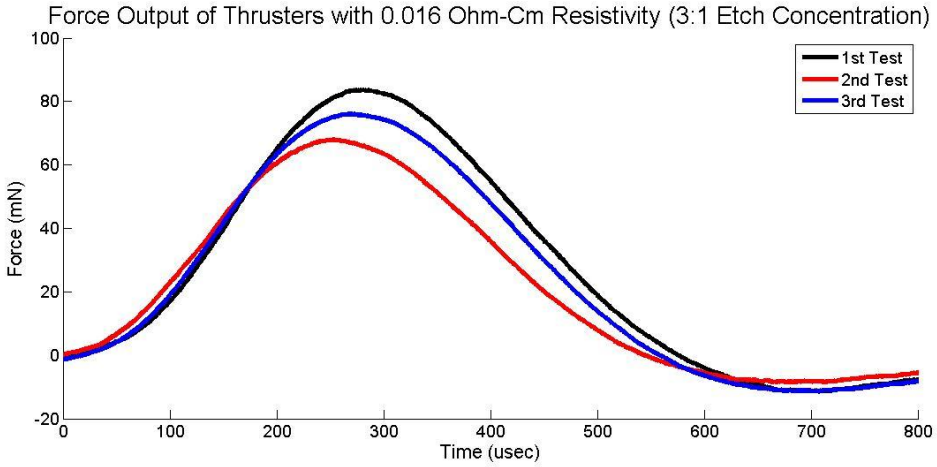

Fig. 10 Output of microthrusters etched at 3:1 ratio with 0.016 ohm-cm resistivity (tests 1–3)

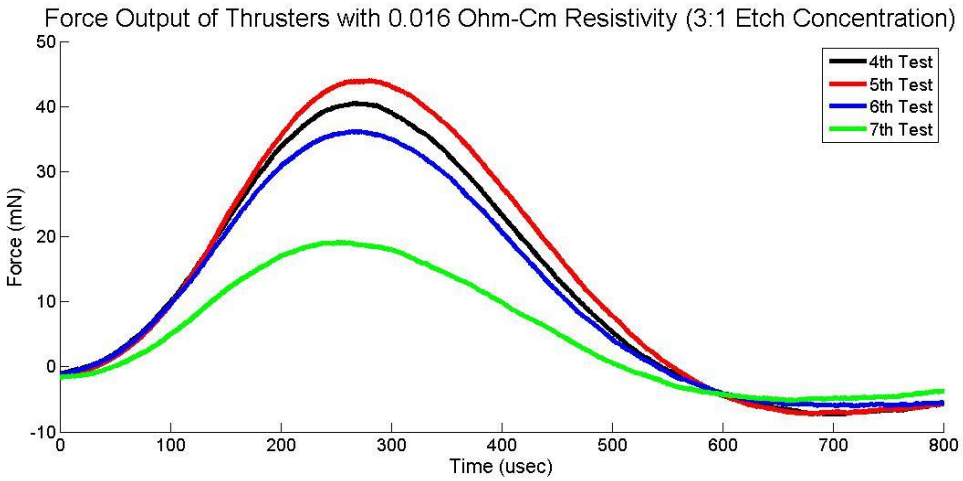

Fig. 11 Output of microthrusters etched at 3:1 ratio with 0.016 ohm-cm resistivity (tests 4–7)

Figures 12 and 13 showcase thrust outputs for etches with a 20:1 concentration for 5.5 ohm-cm and 0.016 ohm-cm resistivity starting wafers, respectively. Keeping resistivity and etch depth constant, a 20:1 etch concentration results in a lower thrust output compared to a 3:1 etch concentration. This is likely due to how the volume of HF and EtOH change the pore morphology of the thruster. However, in order to make any truly conclusive statements, we need to carry out BET tests on actual coupons used for thrust measurements, which is of course complicated by the limited mass available from any given etched coupon.

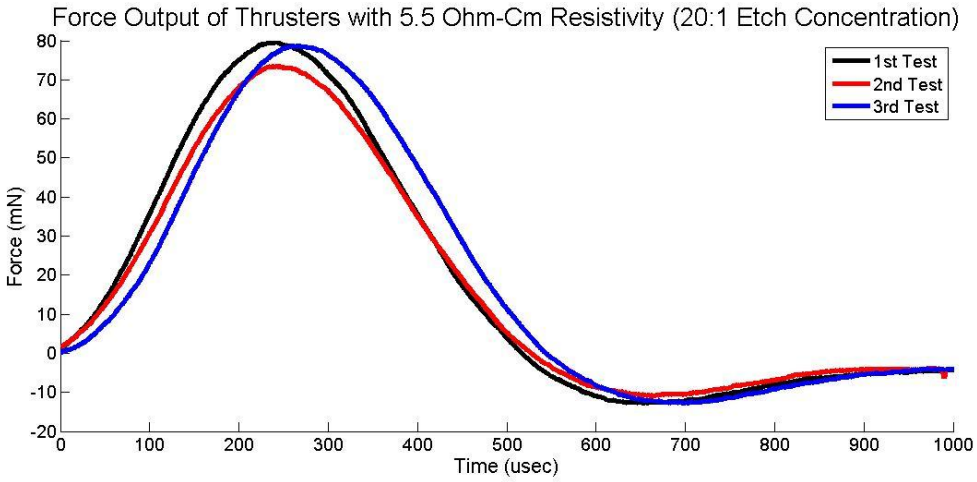

Fig. 12 Output of microthrusters etched at 20:1 ratio with 5.5 ohm-cm resistivity

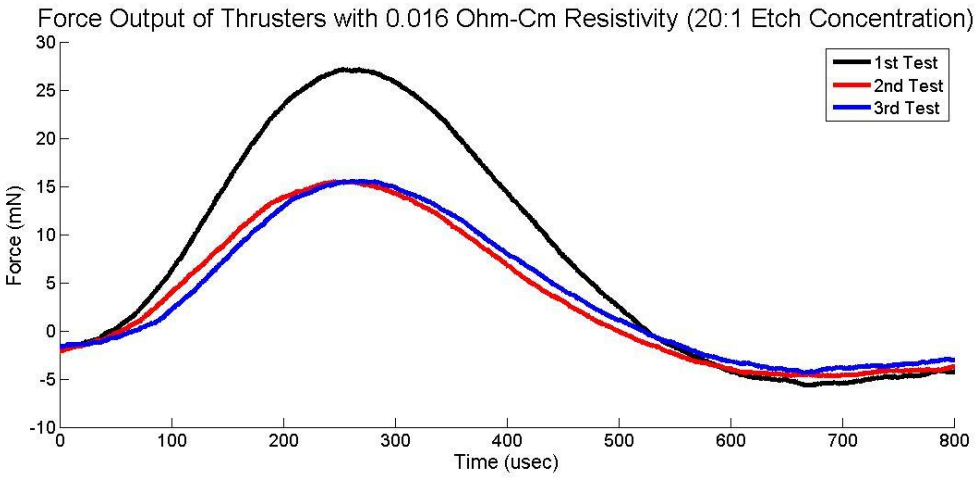

Fig. 13 Output of microthrusters etched at 20:1 ratio with 0.016 ohm-cm resistivity

The variations in thrust magnitude, duration, and estimated impulse are summarized generally in Tables 7 and 8. Impulses were estimated using roughly fit parabolic areas under each force curve, but a more accurate approach would be to actually integrate each force curve. The lower resistivity, 0.016 ohm-cm wafer devices exhibited similar peak force and thrust durations, regardless of etch concentration. The etch time to achieve the same approximate depth also remained constant for these devices. Although it appears that the variation was lower for 20:1 etches compared to 3:1 etches for both 5.5 and 0.016 ohm-cm wafers, it should be noted that the 20:1 etch results only summarize a total of three tests each, while the 3:1 etch results cover 10 and 7 test results for the higher and lower resistivity wafers, respectively. It is possible that larger variations in the 20:1 test results were masked by small sample sets.

We also observed possible symptoms of issues associated with the quality of platinum located on the backside of each wafer, such as pinholes observed after the etch and portions of some wafers with platinum peeling away. These issues may also have contributed to variability in PS morphology and test results. There were also certain instances of "over-etching" or electro-polishing of the pores in the case of the 0.016 ohm-cm wafers, during which etching occurred so quickly that PS did not remain attached to the substrate, resulting in deep, transparent pores. In future work, this problem may be mitigated by reducing the amount of hydrogen peroxide used in the etch solution to reduce the etch rate.

Table 7 Force data of thrusters of 3:1 etch concentrations with 30-micron depth as a function of resistivity

	5.5 ohm-cm	**2.29 ohm-cm**	**0.016 ohm-cm**
Etch Time (minutes)	6	3	2
Thrust (mN)	200–750	50–150	15–80
Thrust Duration (us)	500–1000	800	600
Impulse (mN-s)	0.08–0.5	0.027–0.08	0.007–0.037

Table 8 Force data of thrusters of 20:1 etch concentrations with 30-micron depth as a function of resistivity

	5.5 ohm-cm	**0.016 ohm-cm**
Etch Time (minutes)	3	2
Thrust (mN)	70–80	15–27
Thrust Duration (us)	500	600
Impulse (mN-s)	0.033–0.037	0.007–0.012

5. Conclusion

We have shown that different etch parameters have a great impact on the thrust characteristics of PS-based thrusters, with observed peak forces ranging from 15 to 750 mN. In general, more consistent and repeatable pore morphologies and thrust measurements were obtained when the etch solution was refreshed after each etch and when etches were carried out for longer times. A longer etch time resulted in a deeper etch and more porous material, and the more repeatable pore morphology measurements appeared to correlate with a sample mass of 3 mg or more. The highest thrust levels and longest thrust durations were obtained with 5.5 ohm-cm wafers. Lower resistivity, 0.016 ohm-cm wafer devices exhibited similar peak force and thrust durations, regardless of etch concentration, although these results were lowest in magnitude compared to other wafer resistivities.

Two additional problems may have contributed to variability in results. First, issues associated with the quality of the platinum located on the backside of each wafer from the particular batch of wafers used in this study may have been a problem. The other problem involved working with the lowest resistivity wafers. There were certain instances of "over-etching" or electro-polishing of the pores. Etching occurred so quickly that the PS did not remain in the pores, resulting in deep transparent pores. In future work, we will try to mitigate this problem by reducing the amount of hydrogen peroxide used in the etch when electro-polishing occurs and more carefully documenting any observed experimental differences or unusual outcomes regarding backside platinum conditions or etched PS appearance. In addition, it is imperative to record specific locations of samples used for any measurements in an array of etched devices, in order to provide better accuracy, consistency, and correlation to any variation in the test results.

6. References

1. du Plessis M. Integrated Porous Silicon Nano-Explosive Devices. in Proc. IEEE Symp. Ind. Electron. 2007, pp 1574–1579
2. Currano L, Churaman W, Becker C. Nanoporous silicon as a bulk energetic material. Solid-State Sensors, Actuators and Microsystems Conference, 2009. Transducers 2009. International. pp.2172,2175, 21–25 June 2009.
3. Churaman WA, Gerratt AP, Bergbreiter S, First leaps toward jumping microrobots. Intelligent Robots and Systems (IROS), 2011 IEEE/RSJ International Conference on. pp.1680,1686, 25–30 Sept. 2011.
4. Mukerjee EV, Wallace AP, Yan KY, Howard DW, Smith RL, Collins SD. 2000 Vaporizing liquid microthruster sensors actuators. 2002;83:231–36.
5. Larangot B, Conedera V, Dubreuil P. Solid propellant microthruster: an alternative propulsion device for nanosatellite. 2002, Avignon. Proceedings of the Conference on Aerospace Energetic Equipment, pp.12–14, 10–19.
6. Churaman WA, Morris CJ, Currano LJ, Bergbreiter S. On-chip porous silicon microthruster for robotic platforms. Solid-State Sensors, Actuators and Microsystems (Transducers & Eurosensors XXVII), 2013 Transducers & Eurosensors XXVII: The 17th International Conference on. pp.1599,1602, 16–20 June 2013.

1	DEFENSE TECH INFO CTR
(PDF)	ATTN DTIC OCA
2	US ARMY RSRCH LABORATORY
(PDF)	ATTN IMAL HRA MAIL & RECORDS MGMT
	ATTN RDRL CIO LL TECHL LIB
1	GOVT PRNTG OFC
(PDF)	ATTN A MALHOTRA
4	US ARMY RSRCH LAB
(PDF)	ATTN RDRL SER L R RAMACHANDRAN
	ATTN RDRL SER L W CHURAMAN
	ATTN RDRL SER L D LUNKING
	ATTN RDRL SER L C MORRIS

INTENTIONALLY LEFT BLANK.